PAPER

Check for updates

Effects of hydrogen transport on the kinetic regimes of 4-nitrophenol reduction by sodium borohydride

Tatiana Nizkaia, [iD] [a] Philipp Groppe, [iD] [b] Valentin Müller, [iD] [b] Jens Harting, [iD] [ac] Susanne Wintzheimer [iD] [bd] and Paolo Malgaretti [iD] *[a]

The reduction of 4-nitrophenol (4-NiP) by sodium borohydride is widely used to benchmark heterogeneous catalysts and is commonly simplified as a pseudo-first-order reaction, characterized by a single reaction rate constant. In reality, this reaction is more complex, as it is accompanied by hydrolysis of borohydride and concurrent hydrogenation of 4-NiP by produced hydrogen. This makes the local hydrogen concentration at catalytic sites an important, and so far overlooked, factor in shaping the apparent catalytic activity of heterogeneous catalysts. Re-examining benchmarking experiments on Pt–SiO$_2$ supraparticles with different pore structures, we attribute contrasting kinetic behavior to distinct regimes of hydrogen transport: diffusive transport sustains high local concentrations of hydrogen and pseudo-first-order kinetics of 4-NiP hydrogenation, while bubble-mediated escape causes hydrogen loss, deviations from pseudo-first-order regime and incomplete conversion of 4-NiP. We propose a kinetic model that captures this transition and enables consistent interpretation of experimental data. More broadly, our analysis shows that apparent differences in activity observed in benchmarking experiments that use 4-NiP reduction by borohydride as a test reaction, can arise from hydrogen transport rather than intrinsic properties of the catalyst. This highlights the need to account for the hydrogen transport regime (bubbling/non-bubbling), when comparing catalyst performance across different experiments.

Introduction

The reduction of 4-nitrophenol (4-NiP) by sodium borohydride (NaBH$_4$) in aqueous solutions is widely recognized as a benchmark reaction for evaluating the efficiency of heterogeneous catalysts.[1–4] It has been first described over 20 years ago[5,6] and quickly gained popularity to its operational simplicity and the convenience of *in situ* monitoring using UV-visible spectroscopy. Traditionally, the reaction kinetics have been described as pseudo-first-order, characterized by a single reaction rate constant which depends on initial concentrations of 4-NiP and NaBH$_4$.[7–9]

However, recent studies have shown that this reaction is more complex than previously thought. In fact, the catalysts used for the reaction also promote the hydrolysis of

borohydride, leading to the formation of molecular hydrogen.[10–12] Since this process is much faster than 4-NiP reduction, experiments are typically carried out with a large excess of NaBH$_4$ to ensure complete conversion of 4-NiP and to maintain pseudo-first-order kinetics.[1] Also, some metals can catalyse the hydrogenation of 4-NiP by dissolved hydrogen.[11,13,14] In this case, some of the hydrogen produced by hydrolysis can be used for direct 4-NiP hydrogenation,[11] while the rest is transported away from the catalytic region in the form of bubbles or *via* diffusion, and eventually leaves the reactor. The 4-NiP to 4-AmP conversion rate in this case depends on the balance between hydrogen production and the rate at which it leaves the system, which ultimately depends on the onset of bubbling.[15,16] Accordingly, as it has recently been discussed for other catalytic systems,[17] transport of hydrogen becomes a crucial factor in determining the catalyst efficiency.

While deviations of 4-NiP reduction kinetics from classical models have been observed previously[18–20] and hydrogenation *via* dissolved H$_2$ has been acknowledged,[11] the transport of hydrogen has never been considered as a factor that can affect the reaction kinetics. In this study, we address its relevance by re-examining experimental data on the reduction of 4-NiP using Pt–SiO$_2$ catalytic supraparticles

[a] Helmholtz-Institute Erlangen-Nürnberg for Renewable Energy (IET-2), Forschungszentrum Jülich, Cauerstrase 1, 91058 Erlangen, Germany. E-mail: p.malgaretti@fz-juelich.de
[b] Department of Chemistry and Pharmacy, Friedrich-Alexander-Universität Erlangen-Nürnberg (FAU), Egerlandstrase 1, 91058 Erlangen, Germany
[c] Department of Chemical and Biological Engineering and Department of Physics, Friedrich-Alexander-Universität Erlangen-Nürnberg, Cauerstrase 1, 91058 Erlangen, Germany
*[d] Fraunhofer-Institute for Silicate Research ISC, Neunerplatz 2, 97082 Würzburg, Germany*

(SPs) fabricated *via* spray-drying techniques.[21,22] These SPs offer tunable porosity at a fixed catalyst loading, enabling investigations into how pore size and distribution of the catalyst affect the reaction kinetics. While assessing the catalytic activity of the obtained supraparticles using 4-NiP hydrogenation as a test reaction, we observed puzzling deviations from the expected reaction kinetics, particularly in samples that exhibit bubble formation. To address these deviations, we develop a kinetic model that includes 4-NiP reduction by both sodium borohydride and dissolved H_2, and takes into account the transport of hydrogen. The model reveals two distinct regimes: initially, reduction by borohydride dominates; at later stages, once borohydride is depleted, the main reduction agent is dissolved H_2. We use our model to analyze experimental data and find evidence for H_2-mediated hydrogenation at long times and for the influence of hydrogen transport on the apparent reaction kinetics.

Kinetic model of the two reduction mechanisms

The classical scheme of 4-NiP reduction[7,18,23] describes a binary reaction at the surface of a catalytic metal nanoparticle (M-NP) as:[10]

$$4HO(C_6H_4)NO_2 + 3BH_4^- \overset{M\text{-}NP}{\rightarrow} 4HO(C_6H_4)NH_2 \tag{1}$$
$$+ 3BO_2^- + 2H_2O$$
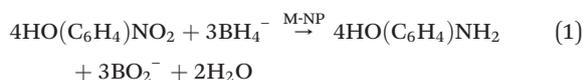
This process is accompanied by catalytic hydrolysis of borohydride,[10]

$$BH_4^- + 4H_2O \overset{M\text{-}NP}{\rightarrow} B(OH)_4^- + 4H_2, \tag{2}$$
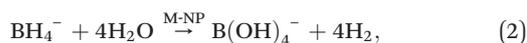
which is typically much faster; hence, an excess of borohydride is required for efficient 4-NiP reduction.[3] Meanwhile, some metals (in particular Pt and Pd) also catalyse a direct hydrogenation reaction with H_2 produced by hydrolysis:[11,13,14]

$$HO(C_6H_4)NO_2 + 3H_2 \overset{M\text{-}NP}{\rightarrow} HO(C_6H_4)NH_2 + 2H_2O, \tag{3}$$

Experimental characterization of this pathway under high H_2 pressure shows its independence on pH and pseudo-zeroth-order kinetics with respect to 4-NiP, up to very small 4-NiP concentrations (see (ref. 13) and the SI in (ref. 11)).

Therefore, two mechanisms can coexist: reduction by sodium borohydride (eqn (1)) and a two-step route *via* hydrolysis and hydrogenation by dissolved H_2 (eqn (2) and (3)). When H_2 is produced, it can either leave the system or be used for 4-NiP hydrogenation. The fraction used is controlled by the competition between the hydrolysis rate and H_2 removal. Accordingly, fast transport reduces the local H_2 concentration and thus the overall conversion rate of 4-NiP. Prior to borohydride depletion, both mechanisms are likely operational, leading to complex reaction kinetics. To capture both chemical pathways together with the transport of hydrogen, we use a simplified kinetic model:

$$\frac{dC_{4\text{-}NiP}}{dt} = -k_A C_{H_2} - 4k_{AB} C_{4\text{-}NiP} C_{NaBH_4}, \tag{4a}$$

$$\frac{dC_{NaBH_4}}{dt} = -k_B C_{NaBH_4} - 3k_{AB} C_{4\text{-}NiP} C_{NaBH_4}, \tag{4b}$$

$$\frac{dC_{H_2}}{dt} = 4k_B C_{NaBH_4} - 3k_A C_{H_2} - \alpha C_{H_2}. \tag{4c}$$

Here, C_{NaBH_4}, $C_{4\text{-}NiP}$, C_{H_2} are concentrations of the respective species, k_{AB} and k_A are effective rate constants of 4-NiP reduction by borohydride and H_2-mediated hydrogenation, k_B is the hydrolysis rate, and α is the H_2 transport rate. Note that these rate coefficients are effective, *i.e.*, they depend on catalyst loading, distribution of catalyst inside the supraparticles, and adsorption kinetics. We remind that we use here a pseudo zeroth order kinetic model for H_2-mediated hydrogenation,[13] which is supposed to break down at very small concentrations of 4-NiP. Our model also neglects the back reaction of 4-AmP with oxygen,[24] which starts to play a role when oxygen adsorbed from the atmosphere dominates over hydrogen produced by hydrolysis: this can happen in the first seconds of the reaction ("induction period") or when the volume of the reaction mixture is very small, resulting in high surface-to-volume ratio. Assumptions and limitations of this model are discussed in more detail in SI.

Incorporating a transport term, αC_{H_2}, into the kinetic model (see eqn (3)) allows us to account for the rate at which hydrogen escapes from the solution. Notably, when hydrogen is released in the form of bubbles, its evacuation rate is significantly higher than in the absence of bubbling, where hydrogen loss is limited to degassing from the liquid surface. To capture changes in the transport mechanism over the course of the reaction, we introduce a simplified, piece-wise constant model for the transport coefficient:

$$\alpha(t) = \begin{cases} \alpha_s & t < t_{bub} \\ \alpha_l & t \geq t_{bub}, \end{cases} \tag{5}$$

where α_s corresponds to bubble-mediated H_2 transport, α_l is the transport coefficient in the absence of bubbles, and t_{bub} is the time at which bubbling stops, which can be determined by visual observation.

The transport coefficient in the absence of bubbling α_l can be estimated as the degassing rate from a stirred beaker: $\alpha_l = k_L a$, where $a = A/V$ is the gas–liquid interfacial area per unit volume, and k_L is the liquid-side mass-transfer coefficient which captures the effective rate of transport of chemical species to the interface.[25] Since α_l is proportional to surface-to-volume ratio, it is not an intrinsic property and depends on the volume of the reaction mixture and on the shape of the reservoir in which the reaction takes place. Accordingly, in order to compare different experimental observations it is important to know (and hence to report) these data.

2186 | *Catal. Sci. Technol.*, 2026, **16**, 2185–2194

This journal is © The Royal Society of Chemistry 2026

On the other hand, bubble-mediated transport coefficient α_s should be regarded as an empirical parameter: the flux of hydrogen in the bubbling regime depends strongly on the conditions of bubble growth and detachment, which are sensitive to the porous structure and wetting properties of the catalyst support, stirring rate, *etc.*

Experimental methods

Synthesis of catalytic supraparticles

In this work, we analyse the kinetics of 4-NiP reduction on three different types of catalytic supraparticles (types A, B, and C):

Type A and type B Pt–SiO$_2$ supraparticles. Catalyst types A and B correspond to the spray-dried Pt–SiO$_2$ supraparticles previously reported by Groppe *et al.*[21] Their synthesis and structural characterization are described in detail in that publication. Briefly, colloidal suspensions containing 4 nm Pt nanoparticles and SiO$_2$ nanoparticles of different sizes in a CaCl$_2$ solution were spray-dried to form hierarchical supraparticles with tunable pore frameworks. Type A supraparticles were prepared from 182 nm SiO$_2$ nanoparticles with varying CaCl$_2$ concentration (0.025–0.075 mmol Ca^{2+}/ g$_{SiO_2}$), producing large interstitial pores (>40 nm). Type B supraparticles were made from 19 nm SiO$_2$ nanoparticles with varying CaCl$_2$ concentration (0.1–0.25 mmol Ca^{2+} g^{-1} SiO$_2$) and feature smaller pores (8–19 nm). The Pt loading, measured *via* inductively coupled plasma atomic emission spectroscopy (ICP AES), for type A and type B particles was similar: 0.9 and 0.94 mg$_{Pt}$/g$_{SiO_2}$, respectively.[21] All structural and compositional data are reproduced from ref. 21 and no additional synthesis or measurements were performed in the present work.

Type C Pt–SiO$_2$ supraparticles. Catalytic supraparticles of type C were newly synthesized following the protocol reported by Groppe *et al.*[22] SiO$_2$ supraparticles were produced by spray-drying an aqueous dispersion of 8 nm SiO$_2$ nanoparticles without CaCl$_2$ to yield compact structures with pore diameters of 2–10 nm. Platinum was subsequently deposited by atomic layer deposition (ALD) conducted on a GEMStar-6 XT ALD reactor from Arradiance using trimethyl(methylcyclopentadienyl) platinum (IV) and ozone as precursors. Two catalyst batches (15 and 30 ALD cycles) were prepared. All ALD and spray-drying parameters were reproduced from ref. 22.

Catalyst stability. For particles of type A and B, stability of the catalyst has been studied in ref. 21. SEM and N$_2$-sorption measurements of the materials after reaction showed no detectable structural degradation (see Fig. S43 and S44, Table S9 in (ref. 21)), and cycle stability tests confirmed reproducible activity over two reaction cycles (see Fig. S45 in (ref. 21)). Moreover, cycle stability tests showed no loss of activity over two consecutive catalytic runs (Fig. S45). A slight activity increase after the second cycle was attributed to minor disintegration of individual Pt nanoparticles, which increases the accessible active surface area. Therefore,

catalyst deactivation can be ruled out as the origin of the deviations from pseudo-first-order kinetics observed in this work. These results indicate that the supraparticle catalysts remain stable under the reaction conditions used in this work.

Reproducibility. The spray-drying fabrication method yields highly reproducible pore structures of the silica supraparticles across independent synthesis batches, confirmed by structural analysis (see Fig. S16 and Table S6 in the SI of (ref. 22)). The ALD-based Pt deposition can show slight batch-to-batch variations regarding the total amount of deposited Pt. However, by quantifying the Pt content using ICP (inductively coupled plasma) measurements, its effects on the apparent fluctuations in the rate constant can be taken into account.

4-NiP reduction experiments

The time-resolved 4-NiP concentration curves for catalysts of type A and B were taken directly from ref. 21 and reanalyzed using the kinetic framework introduced in this study. No new catalytic experiments were carried out for types A or B. For type C catalysts, experiments were performed under identical conditions to those used in Groppe *et al.*:[21] $C_{4\text{-NiP}} = 6.5 \times 10^{-5}$, $C_{NaBH_4} = 0.1M$ in aqueous solution at $T = 25$ °C and pH = 10.4–10.5 set by NaOH addition. The reaction was performed in a 25 mL beaker (30 mm diameter), agitated with a magnetic stirrer at 200 rpm. The reaction was monitored by UV-vis spectroscopy of filtered samples of the reaction mixture, extracted by 2 ml portions at 2 min intervals, starting from the initial volume $V = 20$ ml.[21,22] The decrease in 400 nm absorbance peak corresponding to 4-NiP was used to determine 4-NiP concentration as a function of time:

$$c_{4\text{-NiP}}(t) = \frac{C_{4\text{-NiP}}(t)}{C_{4\text{-NiP}}(0)} = \frac{A(t)}{A(0)}, \tag{6}$$

where $A(t)$ is the amplitude of the peak at time t.[21] The bubbling time was assessed by visual inspection of the video recordings of the experiments.

To assess the importance of H$_2$-mediated reduction, we also performed the experiments for type C particles using gaseous hydrogen as reducing agent. Experiments were performed under the same conditions as described above for 15-cycle Pt ALD on 8 nm SiO$_2$ spherical particles. Reactions were carried out at 25 °C in a 25 mL beaker containing 20 mL of 4-nitrophenol solution (7.5^{-5} M). A 2 mL aliquot was withdrawn at $t = 0$ min, after which H$_2$ was introduced *via* a needle at a flow rate of 10 mL min^{-1}. Successively 2 ml portions have been taken out every 2 minutes to perform UV-vis spectroscopy.

Analysis of experimental data

We revisit here the results of 4-NiP reduction experiments on spray-dried composite Pt–SiO$_2$ supraparticles described in (ref. 21) (type A and B) and complement them with new

measurements for superparticles obtained by spray-drying a dispersion of passive SiO_2 nanoparticles with subsequent incorporation of Pt using the ALD method:[22]

Type A: 182 nm SiO_2 + 4 nm Pt + $CaCl_2$. Large pores (all >40 nm), agglomerates of Pt nanoparticles inside the supraparticles and on the surface; strong bubbling in the first 5–8 min. Dataset from ref. 21.

Type B: 19 nm SiO_2 + 4 nm Pt + $CaCl_2$. Tunable pore size distribution (8–19 nm) with all pores <40 nm; aggregates of Pt particles inside the supraparticles; no bubbling observed. Dataset from ref. 21.

Type C: 8 nm SiO_2 with Pt by ALD[22]. Very small pores (4 nm); small clusters of Pt atoms in a thin layer near the surface of the supraparticle. 4-NiP reduction experiments performed for supraparticles with 15 and 30 ALD cycles show active bubble formation in the initial stage of the reaction: 5–7 min (30 cycles) and 7–9 min (15 cycles). For particles fabricated with 15 ALD cycles, an additional experiment was performed with H_2 as a reducing agent, which was bubbled through the 4-NiP solution at a constant rate of 10 mL min^{-1}.

The evolution of the 4-NiP concentration for supraparticles of types A, B, and C is shown in Fig. 2a, c and e (experimental data are shown as symbols connected by dotted lines). While the initial reaction rates for types A and B are similar, type A particles show weaker activity at longer times and lower 4-NiP conversion after 30 min (see Fig. 2b and d). Type C particles show higher initial reaction rates compared to particles of type A and B, and experience an unexpected surge of activity a few minutes into the reaction (see Fig. 2e and f). Type C particles also exhibit high catalytic activity for the H_2 reduction of 4-nitrophenol (magenta curves in Fig. 2e and f), confirming the viability of the H_2-mediated pathway.
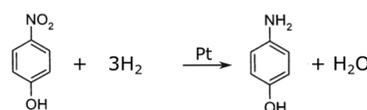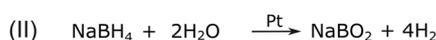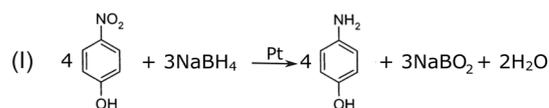
We start by comparing the activity of type A and Type B supraparticles, which all have the same Pt loading. Interestingly, as shown in Fig. 3, some pairs of type A/type B supraparticles exhibit identical catalytic activity during the first 5 min of the reaction, but diverge markedly at longer times. Moreover, Fig. 3 shows that the concentration profiles of type B supraparticles remain linear on a semilogarithmic scale, consistent with pseudo-first-order kinetics, whereas type A profiles deviate after 5–8 min, indicating a transition to a different kinetic regime. To pinpoint this transition, we extract the time evolution of the 4-NiP reduction rate by applying finite-difference differentiation to the measured concentration profile in Fig. 2a, c and e. As shown in Fig. 2b and d at short times ($t < 5$ min), the reaction rates differ between different type A samples, but at longer times ($t > 5$ min), all the rate curves collapse. Notably, while the 4-NiP concentration at t = 5 min varies significantly (Fig. 2a), the rates at and beyond this point are nearly identical (Fig. 2b). This behavior is consistent with the pseudo-zeroth-order kinetics with respect to 4-NiP, characteristic of H_2-mediated hydrogenation reported in ref. 11, 13. This can happen if most of the borohydride is hydrolysed in the first few

minutes of the reaction, after which hydrogenation by dissolved H_2 dominates. This suggestion is also consistent with the fact that production of H_2 bubbles was observed only in the first 5–8 min of the reaction.[21]
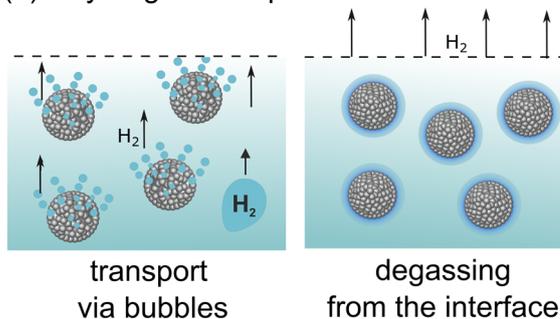
To analyze the data, we use a simple kinetic model eqn ((4a)–(4c)), which describes two pathways of 4-NiP reduction and takes into account hydrogen transport (see SI for details). Before fitting the model to experimental data, we use it to rationalize the observed kinetic features on a qualitative level.

First, our model predicts that for systems with identical reaction rates (k_{AB}, k_A, k_B, see the reaction scheme in Fig. 1 and eqn ((4a)–(4c)) and different transport rates α 4-NiP concentration curves collapse at short times, then diverge at long times to reach different conversion levels (Fig. 4a and b). Indeed, at short times, the reduction by sodium borohydride dominates and the reaction rate is governed by $NaBH_4$ concentration (dashed curve in Fig. 4a and b), which is the same for all the systems; at long times, reduction proceeds *via* dissolved H_2, whose concentration depends on the transport rate. This is exactly what we observe for supraparticles of types A and B with matched initial rates (see Fig. 3). We suggest that these supraparticles show, in fact, very similar catalytic activity, and the difference in their eventual efficiency is due to different mechanisms of hydrogen transport (bubbling *vs.* non-bubbling).

(a) Hydrogenation mechanisms

(I) $4 \begin{array}{c} NO_2 \\ \bigcirc \\ OH \end{array} + 3NaBH_4 \xrightarrow{Pt} 4 \begin{array}{c} NH_2 \\ \bigcirc \\ OH \end{array} + 3NaBO_2 + 2H_2O$

(II) $NaBH_4 + 2H_2O \xrightarrow{Pt} NaBO_2 + 4H_2$

$\begin{array}{c} NO_2 \\ \bigcirc \\ OH \end{array} + 3H_2 \xrightarrow{Pt} \begin{array}{c} NH_2 \\ \bigcirc \\ OH \end{array} + H_2O$

(b) Hydrogen transport

transport via bubbles   degassing from the interface

Fig. 1 (a) Reaction scheme of 4-NiP hydrogenation, depicting different mechanisms: (I) transfer hydrogenation by borohydride and (II) hydrolysis of borohydride and hydrogenation by dissolved hydrogen. (b) Sketch of hydrogen transport mechanisms: bubbling *vs.* degassing from the liquid/gas interface.

Second, our model predicts that catalytic systems can behave differently in the initial stages of the reaction but exhibit the same catalytic activity at long times (collapsing curves in Fig. 2b), if they have the same values of k_A, k_B and α but different values of k_{AB} (Fig. 4c and d). Indeed, in the initial stage, the reaction proceeds mostly via reduction by NaBH$_4$, captured by k_{AB}. However, at later times hydrogenation via H$_2$ becomes dominant. The reduction rate in this region depends only on k_A and the hydrogen concentration c_{H_2}, which, in turn, is defined by the rates of hydrolysis k_B and transport α. The collapse, depicted in Fig. 2b, suggests that supraparticles of type A have the same catalytic activity with respect to hydrogenation by dissolved H$_2$ and hydrolysis, but different catalytic activities with respect to reduction by borohydride.

Finally, the unusual activity surge observed for type C particles is captured by the time-dependent transport $\alpha(t)$ (eqn (5)), with $\alpha_s \gg \alpha_l$ (see Fig. 4e). When bubbling stops before full NaBH$_4$ depletion, H$_2$ produced by hydrolysis accumulates in the solution (see Fig. 4f) and leads to the acceleration of H$_2$-mediated hydrogenation of 4-NiP.

We note that the slowdown of the 4-NiP reduction over time, shown in Fig. 2a, has been observed previously, but was attributed to fractional order reaction kinetics[20] or formation of an intermediate with very high adsorption to the catalyst.[18,19] However, none of these models exhibit naturally the characteristic kinetic features that we have observed in our experiments: namely, the collapse of the reaction rates at long times (due to transition to H$_2$-mediated reduction) and acceleration of the reaction upon cessation of bubbling (due

to accumulation of dissolved H$_2$). Interestingly, we do find these kinetic features in the experimental data we extracted from ref. 18, 20, suggesting that the data reported there is compatible with our model (see SI).

Given these observations, we can fit all the data with eqn (4a)–(4c) and (5) using minimal subsets of fitting parameters, guided by the kinetic features described above. For type A supraparticles, all the curves in Fig. 2a can be fitted with the same values for k_A, k_B, α_s, α_l by solely varying k_{AB}. We use the following set of common parameters:

$$k_B = 7.5 \times 10^{-3}\ s^{-1},\ k_A = 1.45 \times 10^{-7}\ s^{-1},$$

$$\alpha_l = 1.25 \times 10^{-3}\ s^{-1},\ \alpha_s = 4.8 \times 10^{-3}\ s^{-1}, \tag{7}$$

and the following values of bubbling time, based on experimental observations:

$$\text{Type A: } t_{bub} = 7\ \text{min}, \tag{8}$$

$$\text{Type B (non-bubbling): } t_{bub} = 0\ \text{min}. \tag{9}$$

Indeed, the collapse of the reaction rate curves at long times (Fig. 2a) suggests that k_A (H$_2$-mediated hydrogenation rate) and α_l (H$_2$ transport rate in non-bubbling regime) are the same for all curves, and the fact that all curves collapse onto a master curve after the same characteristic time suggests that k_B (hydrolysis rate) and α_s (H$_2$ transport rate in bubbling regime) are the same as well. While other sets of parameters (with different values of k_A, k_B, α_s, α_l for each
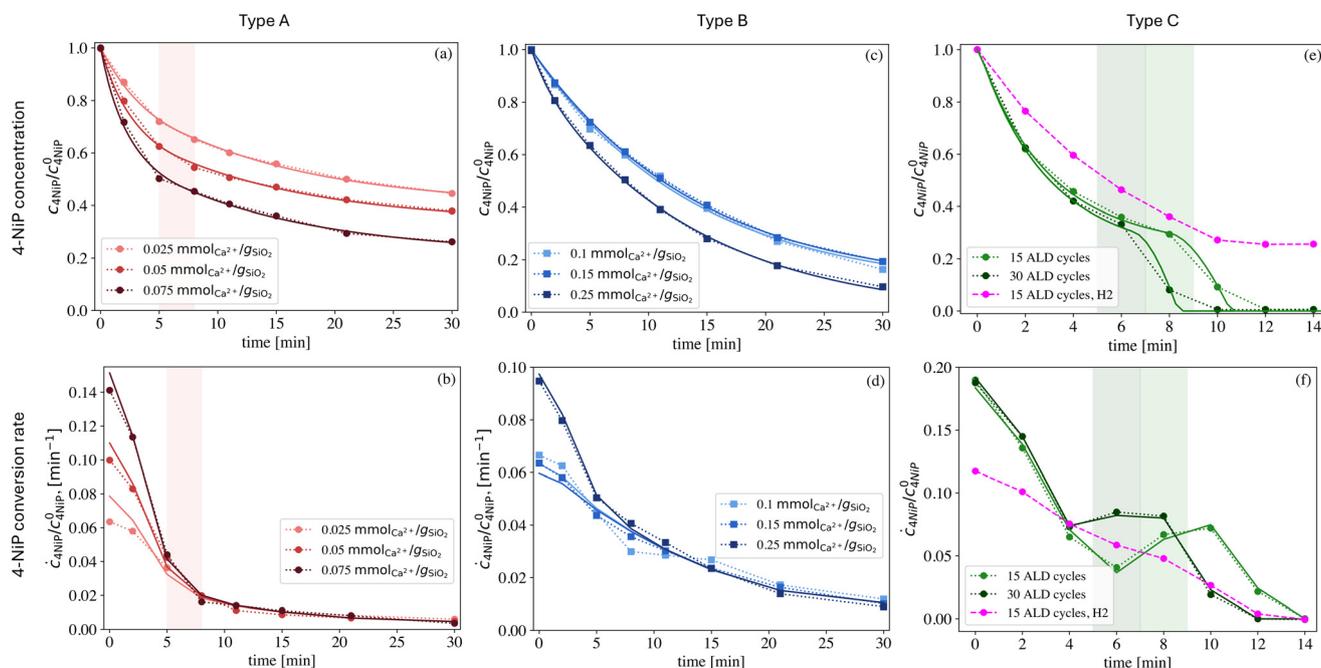
Fig. 2 Experimental data: time evolution of normalized 4-NiP concentration and reaction rate for types A (a and b), B (c and d), and C (e and f). Dotted curves with symbols: experimental data; solid curves: model fits to eqn ((4a)–(4c)). The dashed line in (e and f) corresponds to the experiment on 4-NiP reduction with H$_2$. Shaded areas denote the time range whithin which the bubbling stops.

curve) can also reproduce the data, the observed collapse is unlikely to be coincidental, making a shared set of parameters the most natural explanation. Interestingly, it is possible to fit the data for supraparticles of type B (non-bubbling), using the same set of shared parameters (k_A, k_B and α_l) as for type A supraparticles; however, these fits are not unique because no clear regime change is observed, making multiple mechanisms compatible with the data (see Fig. S1 in the SI).

We remark that the value of α_l, obtained by fitting the tails of the concentration curves, falls well into the expected region for the degassing rate from a stirred beaker: $\alpha_l = 5 \times 10^{-4} \ldots 5 \times 10^{-3} \text{ s}^{-1}$, where we used $k_L = 10^{-5} \ldots 10^{-4} \text{ m sec}^{-1}$ experimentally measured for similar conditions[26,27] and $a = 50 \text{ m}^{-1}$ (for 15 mL of reaction mixture in a 25 mL beaker).

The fitted values of the binary reaction coefficient k_{AB} are provided in Fig. 5. For particles of type A k_{AB} increases with the amount of salt added during supraparticle fabrication. This is in line with the fact that the average size of Pt agglomerates decreases with the increase of $CaCl_2$ concentration,[21] exposing a larger surface area of Pt. However, the collapse of the experimental reduction rate curves at longer times suggests that the amount of catalyst available for H_2-mediated hydrogenation of 4-NiP is the same for all supraparticles. Otherwise we would expect different reaction rates, k_A, for different salt concentrations.

These experimental data are compatible with the assumption that the morphology of the Pt-aggregates mostly affects the surface reaction between 4-NiP and borohydride ions $NaBH_4$ (*i.e.*, k_{AB}), while H_2-mediated hydrogenation (*i.e.*, k_A) and hydrolysis (*i.e.*, k_B) are much less affected. The latter is not so surprising: while the initial steps of multistep hydrolysis reaction are slow at high pH, the subsequent steps are much faster and can proceed in the bulk independently of the catalyst.[11,28,29] This may explain the lack of sensitivity of k_B on the morphology of the Pt-aggregates that we obtain from our analysis.

For what concerns k_A, we recall that 4-NiP has a relatively high adsorption constant to Pt,[7,11] which leads to almost full occupancy of catalysts by 4-NiP, which indeed is the cause of the pseudo zeroth order kinetics of its reaction with H_2. Accordingly, even small amounts of 4-NiP can lead to high occupancy levels of the catalyst, irrespective of the morphology of the Pt-aggregates.

In contrast, borohydride ions have a much smaller adsorption constant,[7] making the transfer hydrogenation rate very sensitive to the local concentration of borohydride, which is affected by the morphology of the aggregates and the ionic strength of the solution.

For supraparticles of type B, the fitted hydrogenation rate constants k_{AB} are close to those for type A, ensuring similar conversion rates at the initial time (see Fig. 5). The drastic difference in long-term behavior between the two types of particles can be captured by changing only one parameter:

the hydrogen transport rate in the initial stage of the reaction: α_s for type A and α_l for type B. However, we stress again that the datasets for particles of type B are compatible with different reaction mechanisms (see Fig. S1 in SI).

For type C supraparticles, the collapse of the reaction curves in the initial stage (Fig. 2e) suggests similar activity with respect to 4-NiP reduction by borohydride. Accordingly, it is possible to fit these curves with the same k_{AB}, k_B, α_s, α_l and different t_{bub}:

$$k_B = 5 \times 10^{-3} \text{ s}^{-1}, \quad k_{AB} = 4.33 \times 10^{-3} \text{ s}^{-1} \text{ L mol}^{-1}, \quad (10)$$

$$\alpha_l = 1.25 \times 10^{-3} \text{ s}^{-1}, \quad \alpha_s = 0.125 \text{ s}^{-1}, \quad (11)$$

its bubbling times estimated from experiment:

$$\text{15 ALD: } t_{bub} = 8 \text{ min} \quad (12)$$

$$\text{30 ALD: } t_{bub} = 6 \text{ min.} \quad (13)$$

The fitted values of hydrogenation rate coefficients for 15 and 30 ALD cycles are very close: $k_A = 1.0 \times 10^{-5} \text{ s}^{-1}$ for particles fabricated with 15 ALD cycles and $k_A = 1.1 \times 10^{-5} \text{ s}^{-1}$ for particles fabricated with 30 ALD cycles. Similar fits, however, could be obtained by fixing k_A and varying k_B or by varying both.

The fits are provided as solid curves in (Fig. 2a–f), with the bottom panels showing finite-difference derivatives of the fits on the experimental time grid. We can see that all the fits are in excellent agreement with the data. Note that the surge of activity observed for type C particles (Fig. 2e and f) is reproduced solely by changing the transport regime from bubbling to non-bubbling at the time deduced from the experiment (visual disappearance of bubbles). To verify our hypothesis and assess the role of hydrogen as reducing agent, we performed an additional experiment with type C particles fabricated with 15 ALD cycles, in which gaseous H_2 was bubbled through a needle submerged in the reaction mixture. While the procedure does not allow to control the actual concentration of dissolved H_2, we can clearly see that H_2-mediated reduction proceeds at a rate comparable to borohydride-driven reduction (see magenta curve in Fig. 2e and f).

Conclusion

By revisiting experimental data on Pt–SiO_2 supraparticles with different pore architectures (types A, B, and C), we suggest that the reduction of 4-NiP by $NaBH_4$ is not governed by a single apparent rate constant but by the interplay of two reaction mechanisms: surface reaction between 4-NiP and borohydride ions on Pt nanoparticles and 4-NiP reduction by H_2 produced in the course of borohydride hydrolysis, which is largely controlled by the conditions of hydrogen transport. At early times, reduction by $NaBH_4$ dominates, while at later

2190 | *Catal. Sci. Technol.*, 2026, **16**, 2185–2194

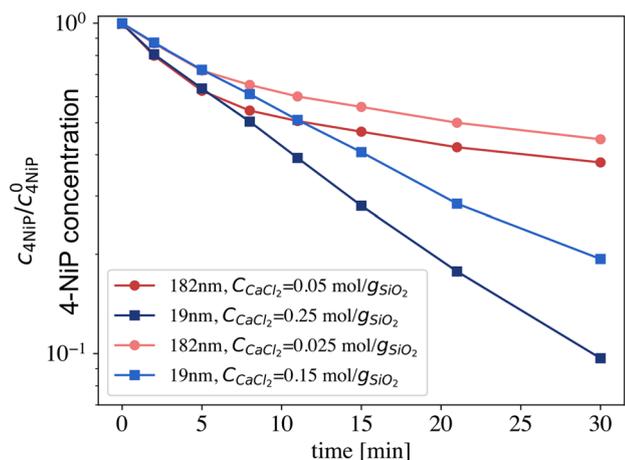This journal is © The Royal Society of Chemistry 2026

Fig. 3 Semi-logarithmic plot of normalized 4-NiP concentration for type A and type B supraparticles with the same initial activity.

times, hydrogenation by dissolved H_2 becomes increasingly relevant once $NaBH_4$ is depleted. Which pathway prevails is determined largely by how fast H_2 is transported out of the system.

The kinetic features demonstrated by supraparticles of type A–C illustrate the combined effect of two reduction mechanisms and hydrogen transport: bubbling accelerates H_2 loss and leads to incomplete conversion (Fig. 2a and 4a), non-bubbling systems sustain pseudo-first-order kinetics and achieve higher conversion (Fig. 2c and 4c), and in some cases, catalytic activity surges once bubbling ceases and dissolved H_2 accumulates (Fig. 2e and f and 4e and f). A

minimal kinetic model combining the two reduction pathways with time-dependent H_2 transport reproduces these observations. The presence of the H_2-mediated reduction mechanism has been confirmed in an independent experiment, in which 4-NiP reduction was achieved by bubbling gaseous hydrogen through the reaction mixture. Moreover, this mechanism can explain previously reported data for which the 4-NiP reduction kinetics deviated from the pseudo first order model and alternative mechanisms, such as fractional reaction order[20] or the presence of intermediates[19] have been proposed. Interestingly, as shown in the SI, these data sets can be easily understood as the outcome of the interplay between the direct 4-NiP reduction *via* $NaBH_4$ and H_2-mediated reduction.

This has important implications for using 4-NiP reduction as a benchmark reaction. First, catalyst performance can only be compared across studies if the hydrogen-transport mechanism is the same; bubbling and non-bubbling systems should not be directly compared. In fact, our analysis shows that supraparticles with essentially identical catalytic activity (same k_A, k_B, k_{AB}) can exhibit very different long-term behavior depending on the rate of hydrogen transport (Fig. 3 and 4a). Second, it is essential to track how the transport regime evolves during the reaction. If bubbling stops before $NaBH_4$ is fully depleted, the concentration of dissolved H_2 rises and triggers a sudden increase in activity (Fig. 2e and 4e). Therefore, in order to disentangle transport effects from intrinsic catalytic activity in benchmarking experiments, it is important to report the hydrogen transport regime (bubbling/non-bubbling) in publications and track its changes throughout the experiment. In non-bubbling regime experiments should be reproduced at different surface-to-

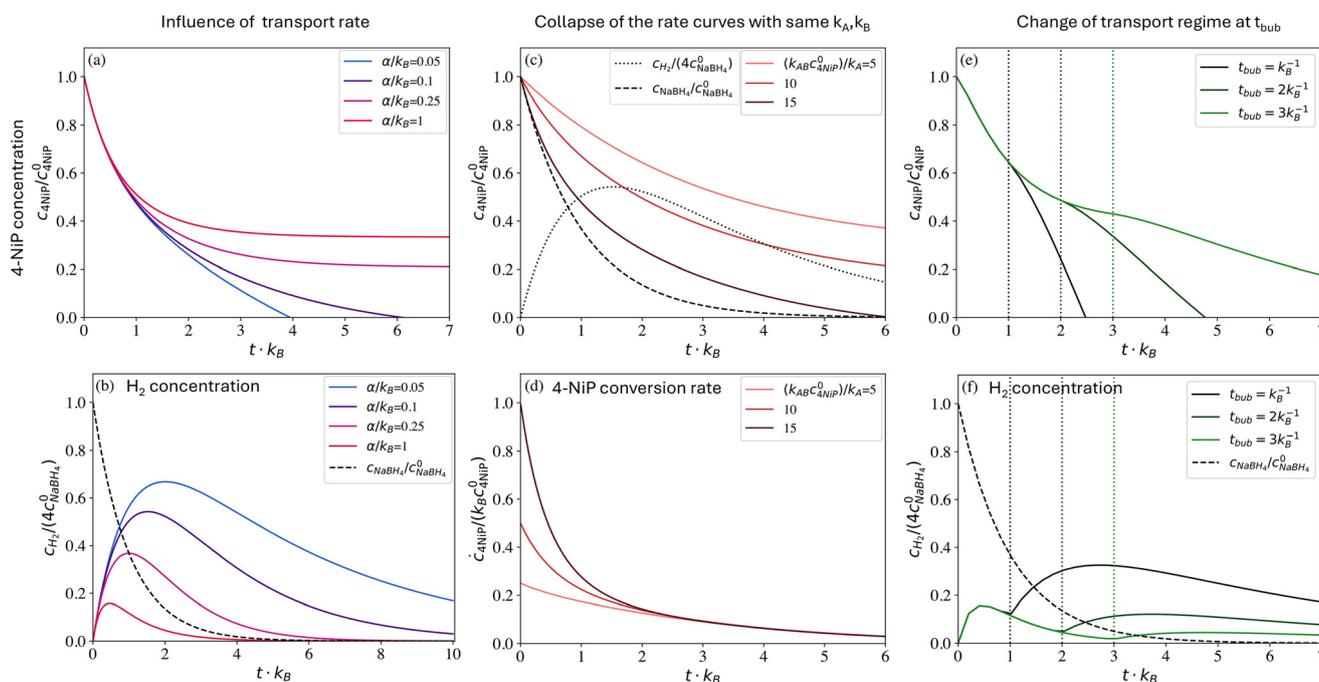**Fig. 4** Theoretical results: calculations using model eqn (4b) and (4c) reproducing typical kinetic features observed in experiments.
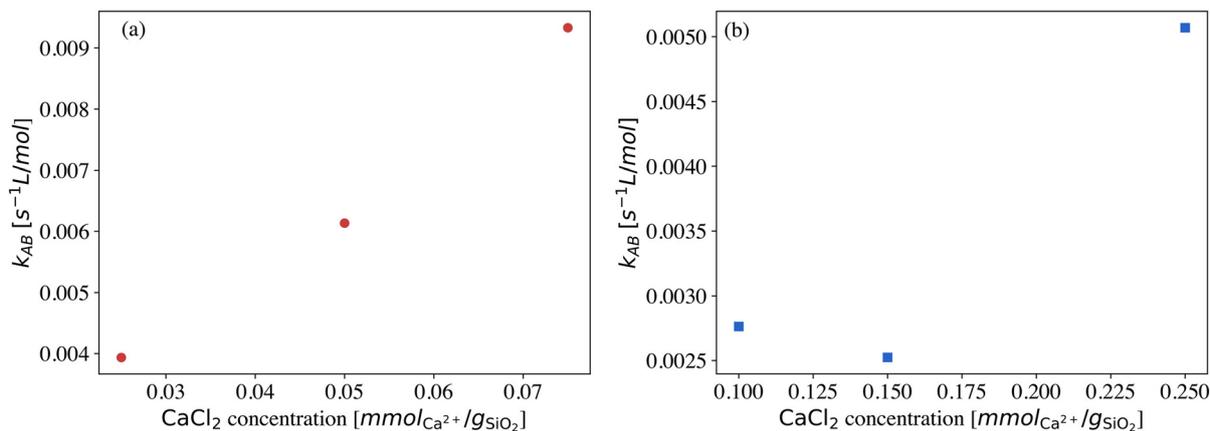
This journal is © The Royal Society of Chemistry 2026

Catal. Sci. Technol., 2026, **16**, 2185–2194 | **2191**

Fig. 5 Fitted values of k_{AB} for supraparticles made of 182 nm (a) and 19 nm SiO_2 supraparticles (b) *versus* salt concentration used during fabrication. Fitting performed using the model eqn ((4a)–(4c)) with parameters defined by eqn (7).

volume ratios (*e.g.* by scaling up the volume of the reaction mixture or by performing the reaction in beakers of different diameters) to exclude the dependency of the results on hydrogen transport rate. Finally, performing additional experiments on direct 4-NiP hydrogenation with H_2 can help to estimate the importance of the H_2-mediated mechanism for a particular catalytic system.

In addition, our analysis illustrates that 4-NiP reduction is not a single reaction but a combination of 4-NiP reduction by borohydride, borohydride hydrolysis, and reduction by dissolved H_2. Catalytic systems may therefore show different activities for each of these reactions. This is evident for type A supraparticles with the same Pt loading but different aggregate sizes: they exhibit the same activity for reduction by dissolved H_2 (see Fig. 2b, long times) but different activities for reduction by borohydride (see Fig. 2b, short times). The balance between the reduction mechanisms also depends on the chemical nature of the catalyst. For example, for silver nanoparticles 4-NiP reduction proceeds almost exclusively *via* binary reaction with $NaBH_4$ at the surface of the catalyst (mechanism I in Fig. 1), because dissolved hydrogen does not adsorb on Ag easily.[10] In contrast, platinum is very active in catalysing both hydrolysis of borohydride and H_2-mediated hydrogenation (mechanism II in Fig. 1),[10] but is also more prone to losses of hydrogen due to bubbling. Interestingly, the highest catalytic activity is often achieved for bimetallic nanoparticles (Ag–Pt,[30] Ni–Pt,[6] *etc.*[31]), which possibly provide an optimal balance between the two mechanisms. A model of 4-NiP reduction as a combination of two reduction mechanisms and hydrogen transport provides a convenient tool to study such systems.

Beyond 4-NiP reduction, our analysis has a broader impact: in generic reduction reactions driven by hydrogen donors, the apparent kinetics can be strongly influenced by hydrogen transport. For example, a dual reduction mechanism similar to the one we described has been reported for formic acid and related donors, where both direct hydride transfer and H_2 production take place.[32–36] This suggests that the transport effects identified here are

not confined to a model system, but are representative of a wider class of transfer hydrogenation reactions. Mechanistic analysis of catalytic performance should therefore account for the fate of *in situ* generated H_2, since it can alter observed kinetics even when the underlying chemistry remains unchanged. Finally, transport effects are expected to play an important role in continuous-flow reactors.[37–41]

Conflicts of interest

The authors declare no conflicts of interest.

Data availability

Published 4-nitrophenol reduction datasets for spray-dried Pt–SiO_2 supraparticles were reanalyzed in this study, while new measurements were carried out only for supraparticles modified by atomic layer deposition (ALD). Full details on data sources, synthesis procedures, and kinetic modeling are provided in the manuscript and the supporting information (SI).

All datasets supporting this article—including the raw 4-nitrophenol concentration time series for types A, B, and C supraparticles and kinetic fitting scripts—are openly available in Zenodo at: https://doi.org/10.5281/zenodo.17607755. Supplementary information is available. See DOI: https://doi.org/10.1039/d5cy01411e.

Acknowledgements

References

1   P. Herves, M. Pérez-Lorenzo, L. M. Liz-Marzán, J. Dzubiella, Y. Lu and M. Ballauff, Catalysis by metallic nanoparticles in aqueous solution: model reactions, *Chem. Soc. Rev.*, 2012, **41**, 5577.

2 M. Goepel, M. Al-Naji, P. With, G. Wagner, O. Oeckler, D. Enke and R. Gläser, Hydrogenation of p-nitrophenol to p-aminophenol as a test reaction for the catalytic activity of supported pt catalysts, *Chem. Eng. Technol.*, 2014, **37**, 551.

3 T. Aditya, A. Pal and T. Pal, Nitroarene reduction: a trusted model reaction to test nanoparticle catalysts, *Chem. Commun.*, 2015, **51**, 9410.

4 T. K. Das and N. C. Das, Advances on catalytic reduction of 4-nitrophenol by nanostructured materials as benchmark reaction, *Int. Nano Lett.*, 2022, **12**, 223.

5 N. Pradhan, A. Pal and T. Pal, Catalytic reduction of aromatic nitro compounds by coinage metal nanoparticles, *Langmuir*, 2001, **17**, 1800.

6 S. K. Ghosh, M. Mandal, S. Kundu, S. Nath and T. Pal, Bimetallic pt–ni nanoparticles can catalyze reduction of aromatic nitro compounds by sodium borohydride in aqueous solution, *Appl. Catal., A*, 2004, **268**, 61.

7 S. Wunder, F. Polzer, Y. Lu, Y. Mei and M. Ballauff, Kinetic analysis of catalytic reduction of 4-nitrophenol by metallic nanoparticles immobilized in spherical polyelectrolyte brushes, *J. Phys. Chem. C*, 2010, **114**, 8814.

8 S. R. Thawarkar, B. Thombare, B. S. Munde and N. D. Khupse, Kinetic investigation for the catalytic reduction of nitrophenol using ionic liquid stabilized gold nanoparticles, *RSC Adv.*, 2018, **8**, 38384.

9 A. Iben Ayad, D. Luart and A. Ould Dris, Kinetic analysis of 4-nitrophenol reduction by "water-soluble" palladium nanoparticles, *Nanomaterials*, 2020, **10**, 1169.

10 S. Varshney, D. Meyerstein, R. Bar-Ziv and T. Zidki, The competition between 4-nitrophenol reduction and bh4-hydrolysis on metal nanoparticle catalysts, *Molecules*, 2023, **28**, 6530.

11 R. Grzeschik, D. Schäfer, T. Holtum, S. Küpper, A. Hoffmann and S. Schlücker, On the overlooked critical role of the ph value on the kinetics of the 4-nitrophenol nabh4-reduction catalyzed by noble-metal nanoparticles (pt, pd, and au), *J. Phys. Chem. C*, 2020, **124**, 2939.

12 A. Serrà, R. Artal, M. Pozo, J. Garcia-Amorós and E. Gómez, Simple environmentally-friendly reduction of 4-nitrophenol, *Catalysts*, 2020, **10**, 458.

13 M. J. Vaidya, S. M. Kulkarni and R. V. Chaudhari, Synthesis of p-aminophenol by catalytic hydrogenation of p-nitrophenol, *Org. Process Res. Dev.*, 2003, **7**, 202.

14 C. Paun, G. S. lowik, E. Lewin and J. Sá, Flow hydrogenation of p-nitrophenol with nanoag/al₂o₃, *RSC Adv.*, 2016, **6**, 87564.

15 A. Oehmichen, L. Datsevich and A. Jess, Influence of bubble evolution on the effective kinetics of heterogeneously catalyzed gas/liquid reactions. part i: Reactions with gaseous products, *Chem. Eng. Technol.*, 2010, **33**, 883.

16 T. Solymosi, M. Geißelbrecht, S. Mayer, M. Auer, P. Leicht, M. Terlinden, P. Malgaretti, A. Bösmann, P. Preuster and J. Harting, et al., Nucleation as a rate-determining step in catalytic gas generation reactions from liquid phase systems, *Sci. Adv.*, 2022, **8**, eade3262.

17 H. H. Heenen, et al., Exploring mesoscopic mass transport effects on electrocatalytic selectivity, *Nat. Catal.*, 2024, **7**, 106.

18 S. Gu, S. Wunder, Y. Lu, M. Ballauff, R. Fenger, K. Rademann, B. Jaquet and A. Zaccone, Kinetic analysis of the catalytic reduction of 4-nitrophenol by metallic nanoparticles, *J. Phys. Chem. C*, 2014, **118**, 18618.

19 S. Gu, Y. Lu, J. Kaiser, M. Albrecht and M. Ballauff, Kinetic analysis of the reduction of 4-nitrophenol catalyzed by au/pd nanoalloys immobilized in spherical polyelectrolyte brushes, *Phys. Chem. Chem. Phys.*, 2015, **17**, 28137.

20 M. Li and G. Chen, Revisiting catalytic model reaction p-nitrophenol/nabh 4 using metallic nanoparticles coated on polymeric spheres, *Nanoscale*, 2013, **5**, 11919.

21 P. Groppe, J. Reichstein, S. Carl, C. Cuadrado Collados, B.-J. Niebuur, K. Zhang, B. Apeleo Zubiri, J. Libuda, T. Kraus and T. Retzer, et al., Catalyst supraparticles: Tuning the structure of spray-dried pt/sio2 supraparticles via salt-based colloidal manipulation to control their catalytic performance, *Small*, 2024, 2310813.

22 P. Groppe, V. Müller, J. Will, X. Zhou, K. Zhang, M. S. Moritz, C. Papp, J. Libuda, T. Retzer and E. Spiecker, et al., Atomic layer deposition on spray-dried supraparticles to rationally design catalysts with ultralow noble metal loadings, *Chem. Mater.*, 2025, **37**, 2815.

23 S. Saha, A. Pal, S. Kundu, S. Basu and T. Pal, Photochemical green synthesis of calciumalginate-stabilized ag and au nanoparticles and their catalytic application to 4-nitrophenol reduction, *Langmuir*, 2010, **26**, 2885.

24 E. Menumerov, R. A. Hughes and S. Neretina, Catalytic reduction of 4-nitrophenol: a quantitative assessment of the role of dissolved oxygen in determining the induction time, *Nano Lett.*, 2016, **16**, 7791.

25 P. V. Danckwerts et al., *Gas-liquid reactions* McGraw-Hill New York, 1970.

26 A. Cents, F. De Bruijn, D. W. F. Brilman and G. Versteeg, Validation of the danckwerts-plot technique by simultaneous chemical absorption of co2 and physical desorption of o2, *Chem. Eng. Sci.*, 2005, **60**, 5809.

27 E. S. Hamborg, S. R. Kersten and G. F. Versteeg, Absorption and desorption mass transfer rates in non-reactive systems, *Chem. Eng. J.*, 2010, **161**, 191.

28 R. E. Mesmer and W. L. Jolly, The hydrolysis of aqueous hydroborate, *Inorg. Chem.*, 1962, **1**, 608.

29 F. T. Wang and W. L. Jolly, Kinetic study of the intermediates in the hydrolysis of the hydroborate ion, *Inorg. Chem.*, 1972, **11**, 1933.

30 S. Varshney, R. Bar-Ziv and T. Zidki, On the remarkable performance of silver-based alloy nanoparticles in 4-nitrophenol catalytic reduction, *ChemCatChem*, 2020, **12**, 4680.

31 Z. D. Pozun, S. E. Rodenbusch, E. Keller, K. Tran, W. Tang, K. J. Stevenson and G. Henkelman, A systematic investigation of p-nitrophenol reduction by bimetallic dendrimer encapsulated nanoparticles, *J. Phys. Chem. C*, 2013, **117**, 7598.

This journal is © The Royal Society of Chemistry 2026

Catal. Sci. Technol., 2026, **16**, 2185–2194 | **2193**

32 D. A. Berry, A. Smith, M. E. Jones and D. G. Blackmond, An expanded catalytic cycle for the transfer hydrogenation of ketones with formic acid, *Faraday Discuss.*, 2019, **220**, 45.

33 R. Nie, X. Jin, X. Chen and G. Lu, Recent advances in catalytic transfer hydrogenation with formic acid, *ACS Catal.*, 2021, **11**, 524.

34 Y. Zhang, W. Li, F. Li, J. Li, W. Xue, M. Zhao and Y. Wang, Synthesis of p-aminophenol by transfer hydrogenation of nitrobenzene with formic acid as a hydrogen source: effect of pt loading and solid acid type, *New J. Chem.*, 2024, **48**, 664.

35 Z. Yu and J. Spencer, Catalytic transfer hydrogenation with formic acid over supported metals: evidence for a direct pairwise hydrogen transfer pathway, *Chem. Commun.*, 1998, 1993.

36 R. Javaid, T. Yamaguchi, A. Tanimu, A. Fayyaz, T. Kimura and N. Itoh, Continuous-flow hydrogenation of p-nitrophenol with formic acid over pd-coated microreactors, *Beilstein J. Org. Chem.*, 2013, **9**, 2109.

37 A. I. Elhadad and M. Luty-B locho, Safety and process intensification of catalytic reduction of 4-nitophenol using sodium borohydride in flow microreactor system, *Catalysts*, 2025, **15**, 1038.

38 A. Iben Ayad, E. Guénin and A. Ould Dris, Continuous flow reduction of 4-nitrophenol by "water soluble" palladium nanoparticles: from batch to continuous flow system, *J. Flow Chem.*, 2022, **12**, 101.

39 J. Park, J. S. Maier, C. Evans, M. Hatzell, S. France, C. Sievers and A. S. Bommarius, Simultaneous hydrogenation and acetylation of 4-nitrophenol to paracetamol in a two-stage packed-bed reactor, *ACS Sustainable Chem. Eng.*, 2025, **13**, 5906.

40 V. Lomonosov, A. Popova, O. Gubanova, V. Nevedomskiy, A. Garshev, S. Cherepanova, P. Gushchin, A. Nechaev and S. Varfolomeev, Solvent effects on the kinetics of 4-nitrophenol reduction by nabh4 in the presence of ag and au nanoparticles, *React. Chem. Eng.*, 2022, **7**, 1109.

41 M. Ali, S. Kumar, R. Patel, N. Verma and A. Singh, Advances in 4-nitrophenol detection and reduction methods and materials, *ACS Omega*, 2024, **9**, 12345.

2194 | *Catal. Sci. Technol.*, 2026, **16**, 2185–2194

This journal is © The Royal Society of Chemistry 2026